Impact of oxygen content on debinding of binder jetted 17-4 PH stainless steel: Part II - Sintering

Research Article

I·M3 Institute of Materials, Minerals & Mining

Powder Metallurgy
2025, Vol. 68(1) 16–28

DOI: 10.1177/00325899241307871
journals.sagepub.com/home/pmg

Impact of oxygen content on debinding of binder jetted 17-4 PH stainless steel: Part II – Sintering

Kai Zissel[1,2], Elena Bernardo[2], Pierre Forêt[2] and Eduard Hryha[1]

Abstract

Binder jetting requires the sintering of green parts to reach the properties of a metallic component. The sintering activity and sintered material properties of stainless steels are sensitive to powder oxidation and binder contamination, which are introduced by improper debinding. Air is often used during thermal debinding as oxygen aids binder removal, but the metal powder is oxidised being detrimental to sintering densification and final material properties. Hence, the impact of decreasing oxygen content in the debinding atmosphere on the sintering of 17-4 PH at 1300°C for 2 h in an inert argon atmosphere was investigated. Debinding in oxygen-containing atmospheres revealed the presence of δ-ferrite in the sintered microstructure, enhancing densification during sintering. Debinding in an inert Ar atmosphere resulted in low densification that was correlated to the absence of δ-ferrite due to the high amount of carbon in the sintered part. The high carbon content after debinding in Ar resulted in nearly complete oxygen removal by carbothermal reduction during sintering. Debinding in Ar + 1 vol.% O_2 achieved the best combination of reducing final oxygen content by 46% via carbothermal reduction and the absence of carbon pickup during debinding and sintering. Debinding in processing atmospheres containing 3 vol.% O_2 up to 20 vol.% O_2, in contrast, led to a significant oxygen increase of 53 to 74% after sintering compared to the virgin powder.

Keywords

binder jetting, debinding, sintering, processing atmosphere, oxidation, carbothermal reduction, 17-4 PH, stainless steel

Received: 26 June 2024; accepted: 22 November 2024

Introduction

Binder jetting (BJT) emerged as a potential cost-efficient and highly productive additive manufacturing technology for the production of complex metal components compared to other powder bed additive manufacturing technologies. The printing process, where a liquid binder is jetted onto a powder bed in a layer-wise fashion, enables the shaping of intricate geometries and features. The powder packing in the green parts typically reaches densities of 50%–60% relative to the bulk material.[1] As the loose powder compact is only glued together by the binder, the green parts have no technical application. Only by sintering the green parts, the necessary strength for technical applications is generated. Sintering is, therefore, one of the most crucial aspects of the BJT process chain, as it determines the final material properties and final dimensions of the manufactured part.

For successful sintering and hence efficient densification and strengthening of the green compact, two prerequisites need to be ensured. First, the organic binder located between the powder surfaces needs to be removed, which is termed debinding. Second, the removal of the natural oxide layer covering the metal powder surface is a prerequisite for the formation of strong sintering necks, as oxides inhibit material transport between particles and therefore sintering.[2,3] The removal of the binder and the reduction of the surface oxide layer are both strongly influenced by the surrounding processing atmosphere. Debinding and sintering can be combined into one thermal cycle but can be separated for several reasons. Efficient debinding might require a different atmosphere than sintering. Furthermore, debinding products contaminate the required high-purity sintering atmospheres and may

[1]Department of Industrial and Materials Science, Chalmers University of Technology, Gothenburg, Sweden
[2]Linde GmbH, Unterschleißheim, Germany

Corresponding author:
Kai Zissel, Department of Industrial and Materials Science, Chalmers University of Technology, Rännvägen 2A, Gothenburg 412 96, Sweden.
Email: zissel@chalmers.se

increase the wear of sensitive and expensive furnace equipment.

The changes in the powder surface chemistry and binder residuals from the green part to the brown part during debinding will influence the subsequent sintering process. Simple binder removal concepts rely solely on slow heating in ambient air for long processing times, as oxygen (O_2) aids binder decomposition.[4] The major drawback is that the metal powder is prone to oxidation, especially at high debinding temperatures. The debinding in air is effective for iron, copper and nickel because the powder oxidation can mostly be reversed by subsequent sintering in hydrogen (H_2) to reduce metal oxides.[4] Although debinding and sintering in a pure hydrogen atmosphere is effective in reducing metal oxides, safety concerns, high prices and local regulations might limit its use.[5] Consequently, for sintering in inert or slightly reducing atmospheres, the oxidation of the metal powder during debinding needs to be minimised. Oxidation becomes especially problematic for metals, which form stable oxides such as stainless steels, aluminium or titanium alloys.[4]

Stainless steels are a widely adopted material class for BJT, which are sensitive to oxygen as well as carbon content. One of the most used stainless steels in BJT is 17-4 PH because it provides a good combination of mechanical performance and corrosion resistance. Difficulties in the sintering of 17-4 PH emerge from variations in the alloy composition and especially from retained carbon and oxygen.[6] For 17-4 PH, a low residual carbon content, preferably below 0.1 wt.%, is targeted to ensure a good combination of strength, hardness and corrosion properties.[6–8] Sources of carbon are the powder itself and the sacrificial binder, which can add carbon during its decomposition.[6] Compositional specifications for 17-4 PH often do not include oxygen,[6] but oxygen inclusions are detrimental to the mechanical properties of stainless steels. 17-4 PH contains a high amount of Cr (15.5–17.5 wt.%) and considerable amounts of Si ($\leq$1.0 wt.%) and Mn ($\leq$1 wt.%).[9] These elements form stable oxides, which are difficult to remove during sintering. Sources of oxygen are the powder itself, the binder, binder decomposition products and the processing atmosphere.[6]

Extensive research on steels containing oxidation-sensitive elements processed by the powder metallurgy (PM) route highlighted the importance of powder surface reactions during debinding and sintering.[10–19] The atmosphere interaction of the powder is crucial since the surface area of a powder compact is about 10,000 higher than the surface area of a bulk material having the same mass.[5] The formation of strong inter-particle bonds is crucial for high mechanical performance of sintered components.[5] The transformation of iron oxides into more stable oxides (Cr, Mn and Si) is problematic and might already occur at temperatures below 700°C.[20] The critical stage is during heating between 800°C and 1000°C because surface oxides get entrapped in the growing inter-particle bonds and iron oxides continue to transform into more stable oxides.[14] Once formed, stable oxides require high temperatures, low oxygen partial pressures and reducing agents to be removed. Danninger et al. demonstrated in early works the necessity of sintering at high temperature for deoxidation of Cr alloy steels.[21,22] From a thermodynamic perspective, an increase in temperature is required to assure necessary thermodynamic conditions for the reduction of more stable Cr-rich oxides due to the decrease in oxide stability with increasing temperature, as described in detail elsewhere.[2,12]

Consequently, a low initial oxygen content in the brown part needs to be achieved for sintering while removing the binder efficiently. The debinding process is crucial since it determines the amount of residual binder and powder oxidation in the brown part. Tailoring the oxygen content in the debinding atmosphere was explored in the first part of the study to balance binder residue, powder oxidation and brown part brittleness.[23] Debinding in inert Ar resulted in high binder residue and low powder oxidation.[23] Debinding in 3 vol.% O_2 to 20 vol.% O_2 allowed to remove the binder almost completely, which increased the brittleness of the brown parts and led to minor powder losses during handling.[23] In addition, the powder showed strong oxidation after debinding. The best combination of low binder residue, lower powder oxidation and sufficient brown part strength was achieved for debinding in Ar + 1 vol.% O_2.[23]

This study aimed to assess the impact of the oxygen content in the debinding atmosphere on subsequent sintering densification, microstructure and bulk chemistry of binder jetted 17-4 PH stainless steel parts. The sintering was conducted at 1300°C for 2 h in an inert argon atmosphere. An inert atmosphere was chosen due to two reasons. First, the influence of the binder residue products, determined by the debinding atmosphere used, should not be affected by reactive species provided by the sintering atmosphere. Second, the potential of combining a low oxygen-containing debinding atmosphere with sintering in an inert Ar or lean-reducing atmosphere is an economically attractive alternative to hydrogen sintering.

The green parts were debinded in a variety of debinding atmospheres including inert Ar, Ar + 1 vol.% O_2, Ar + 3 vol.% O_2, Ar + 4 vol.% O_2 + 5 vol.% CO_2, Ar + 8 vol.% O_2 and N_2 + 20 vol.% O_2 as described in detail in part I of this study.[23] The obtained brown parts were the basis for the sintering trials in this work. The effect of oxygen content in the debinding atmosphere was assessed by density, shrinkage, microstructure and final material chemistry. The aim was to further provide an in-depth investigation of the chemical evolution from virgin powder to green part, followed by brown part and finally to sintered part in dependence of the debinding atmosphere.

Materials and methods

Materials and printing

The 17-4 PH stainless steel virgin powder (Desktop Metal, USA) used in this study was nitrogen atomised. The composition of the 17-4 PH powder used is provided in

Table 1. Elemental composition of the 17-4 PH stainless steel powder in wt.%.

Cr	Ni	Cu	Mn	Si	Nb + Ta	Co	N	Mo	O	C
17.77	4.15	3.95	0.46	0.56	0.29	0.04	0.25	0.05	0.116	0.024

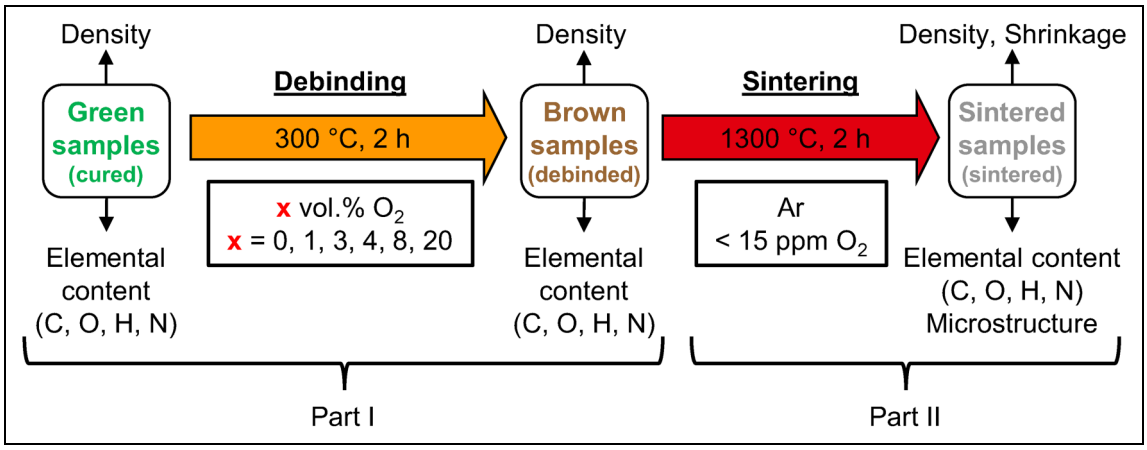

Figure 1. Experimental flow chart displaying thermal processing and material characterisation for the debinding and sintering study.

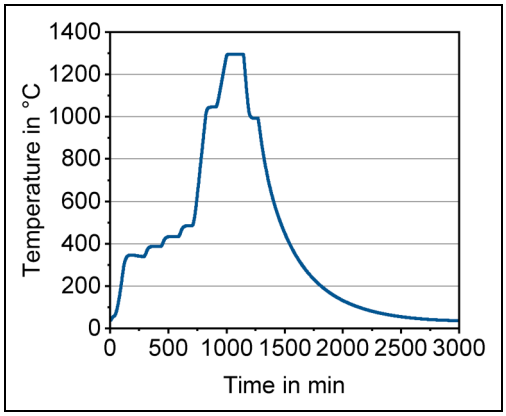

Figure 2. Thermal cycle measured by a thermocouple placed near the 17-4 PH samples inside the furnace.

Table 1. The particle size distribution was determined to be $D_{10} = 6.5$ µm, $D_{50} = 15.3$ µm, and $D_{90} = 28.2$ µm. The powder density determined by a He pycnometer was 7.82 g/cm³. A binder on water basis (SPJ-04, Desktop Metal, USA) was applied for printing on a Production System P-1 (Desktop Metal, USA). The binder contains solvents and a thermoset polymer. Cuboid samples with dimensions of $10 \times 10 \times 10$ mm³ were printed. Additionally, cylinders with a diameter of 2.9 mm and a height of 11.9 mm were printed for chemistry measurements. Further details on the printing process and parameters are described in Part I.[23]

Curing of the green parts was performed at 200°C for 4 h in a furnace under forced air convection (TR 120 LS, Nabertherm GmbH, Germany). Afterward, the samples were removed in the depowdering step by employing brushes and compressed air.

Thermal debinding and sintering

In the first part of this study, green parts were debinded at 300°C for 2 h in atmospheres with different oxygen content.[23] The chosen debinding atmospheres were Ar, Ar + 1 vol.% O_2, Ar + 3 vol.% O_2, Ar + 4 vol.% O_2 + 5 vol.% CO_2, Ar + 8 vol.% O_2 and N_2 + 20 vol.% O_2 at a constant flow of 4 l/min. The obtained brown samples were used for the sintering trials in this work. The brown parts were sintered at 1300°C for 2 h in Ar. A schematic illustration of the experimental procedure for debinding and sintering is given in Figure 1.

One cuboid and one cylindrical brown part from each of the six debinding atmospheres were randomly placed close to each other on a ceramic setter and sintered together in the same furnace cycle. The thermal cycle for debinding and sintering of samples prior debinded at 300°C contained several holding segments at 350°C, 400°C, 450°C and 500°C to ensure uniform heating of components and defect-free residual binder removal. The subsequent heating rate was 5°C/min with a holding step at 1050°C for 1 h for oxide removal. The final sintering temperature of 1300°C was reached with a heating rate of 3°C/min. A solution annealing step was introduced after sintering. The actual temperature was measured inside the furnace close to the samples and is plotted in Figure 2. Natural cooling took place in the furnace after sintering.

The sintering was conducted three times amounting to three sintered cuboid specimens and three sintered cylinders per debinding atmosphere to validate the repeatability of the results. The sintering was performed in an inert Ar atmosphere to ensure that only the impact of the debinding atmosphere was analysed by not introducing reactive components through the sintering atmosphere. In addition, the effectiveness of sintering in Ar in combination with a tailored

debinding atmosphere for binder jetted 17-4 PH green parts at 1300°C for 17-4 PH was investigated. The purity of the atmosphere (<15 ppm O_2) was ensured by measuring the oxygen content in the off-gas of the furnace.

Material characterisation

The densities after sintering were determined by three methods. First, the sintered densities were calculated by the weight and the volume of the samples. The volume of the cuboid specimens was calculated by measuring the *X*, *Y* and *Z* dimensions using a micrometre screw gauge with an accuracy of ±1 µm. The *X* direction corresponded to the powder spreading direction and printing direction. The *Y* direction was perpendicular to the powder spreading direction. The *Z* direction corresponded to the build direction. The measured dimensions were also utilised to calculate the shrinkage after sintering compared to the green part dimensions. Second, the density of the sintered specimen was assessed by Archimedes' principle. Third, the samples were cut and metallographically prepared by grinding and polishing to assess the porosities in the *XZ* and *XY* plane by light optical microscopy (VHX-6000, Keyence, Germany). The porosity was determined by the image analysis software Fiji using the thresholding method. For all three measurement techniques, the arithmetic mean of three cuboid specimens per debinding atmosphere was calculated. After porosity analysis, the cross-sections were etched with Kalling's reagent to reveal microstructural features.

The inert gas fusion technique (ONH836, LECO Corporation, USA) was utilised to analyse the oxygen, nitrogen and hydrogen contents of the samples. Three cylindrical samples after sintering were measured per debinding atmosphere. For carbon analysis, the inert gas fusion method (CS 2000, ELTRA GmbH, Germany) was also used. The three measurements per debinding atmosphere were performed from a cut half of the cuboid specimen. Based on the elemental composition of the 17-4 PH powder, thermodynamic calculations (ThermoCalc 2019b, Thermo-Calc Software AB, Sweden) using the database TCFE9 Steels/Fe-alloys were performed to calculate equilibrium phases and corresponding phase fractions present during the sintering process with varying carbon content.

Results and discussion

Sintered density and shrinkage

The density and shrinkage determined after sintering are simple indicators of the sintering activity. The obtained densities after sintering at 1300°C for 2 h in Ar are shown in Figure 3 depending on the debinding atmosphere. The relative densities were calculated based on the powder density of 7.82 g/cm³. Note that the mean values and standard deviations stemmed from three separate sintering cycles containing samples from each debinding atmosphere.

Debinding in Ar led to a significantly lower sintered density by ~5% (0.4 g/cm³) compared to the green parts debinded in oxygen-containing atmospheres. The densities after sintering were comparable for debinding from 1 vol.% O_2 to 20 vol.% O_2, all in the range between ~92.5% and ~95%. The densities measured by Archimedes' principle showed the same trend but tended to be slightly higher than the volume-based densities. This could be attributed to the surface roughness, which is not accounted for when measuring with a calliper or micrometre screw gauge[24], and the effect of open porosity.

The densities determined by light optical microscopy (LOM) measurements for the *XZ* and *XY* planes are plotted in Figure 4. The areal density after debinding in Ar was considerably lower at ~88% than for debinding in oxygen-containing gas mixtures. With the addition of 1 vol.% O_2 to the debinding atmosphere, the sintered density increased significantly to ~98%. The debinding in 3 vol.% O_2 to 20 vol.% O_2 resulted in similar densities between ~97% and ~98%. The optical measurements

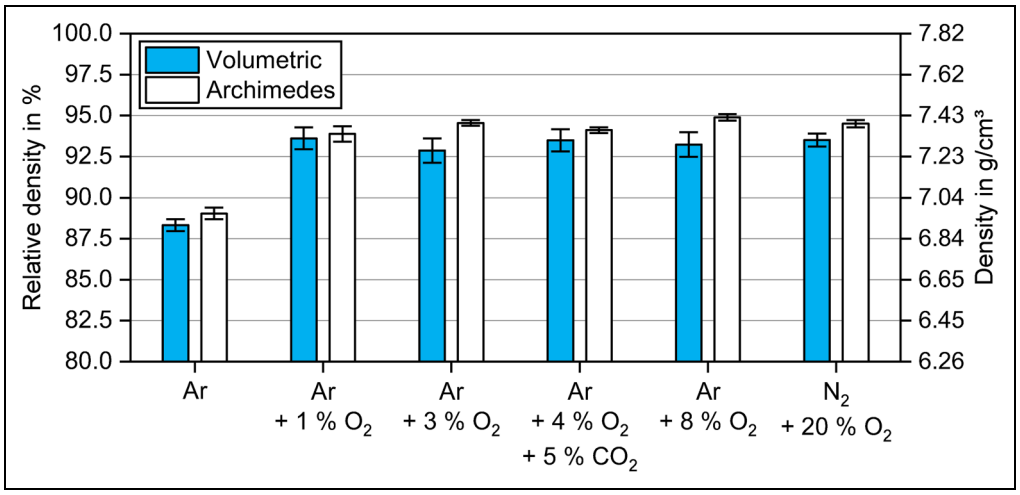

Figure 3. Densities of samples debinded in atmospheres with different oxygen content at 300°C for 2 h and sintered in Ar at 1300°C for 2 h measured by volume calculation and Archimedes' principle.

confirmed the trend seen in Figure 3. In general, the porosity in the *XZ* plane tended to be up to ~1% higher than in the *XY* plane. This can be attributed to the higher porosity created in the *XZ* plane in the green part between each deposited powder layer, which is typical for the BJT printing process.[24–27]

The density determined by LOM was higher than the relative density, which was based on the 17-4 PH powder density of 7.82 g/cm³. The porosity observed via LOM is a better indicator of density because it is not affected by the bulk density of the sintered material. The bulk density of the material can range from 7.66 to 8.00 g/cm³ and is influenced by present phase fractions and the elemental composition after sintering.[8] The MPIF 35 and ASTM B883-24 standards for metal injection moulding of 17-4 PH define a typical density of 7.5 g/cm³.[28,29] Therefore, it can be argued that the actual bulk density of the material is lower than the powder density.

In Figure 5, the shrinkages of samples debinded in atmospheres with different oxygen content and sintered in Ar at 1300°C are shown for the *X*, *Y* and *Z* directions. Note that the mean values and standard deviations were based on three sintering runs containing every debinding atmosphere. Overall, shrinkages after debinding in Ar were the lowest. This was linked to the lowest sintered densities. Consequently, higher and comparable shrinkages were found for the oxygen-containing debinding atmospheres as higher densities were obtained compared to debinding in Ar.

Seemingly higher shrinkages despite comparable densities for oxygen-containing atmospheres can be explained by several factors. The increased brown part brittleness for samples debinded in 3 vol.% O_2 to 20 vol.% O_2 resulted in powder loss during handling affecting final dimensions. This was especially evident for the shrinkage in the *Z* direction for debinding in N_2 + 20 vol.% O_2. In addition, the

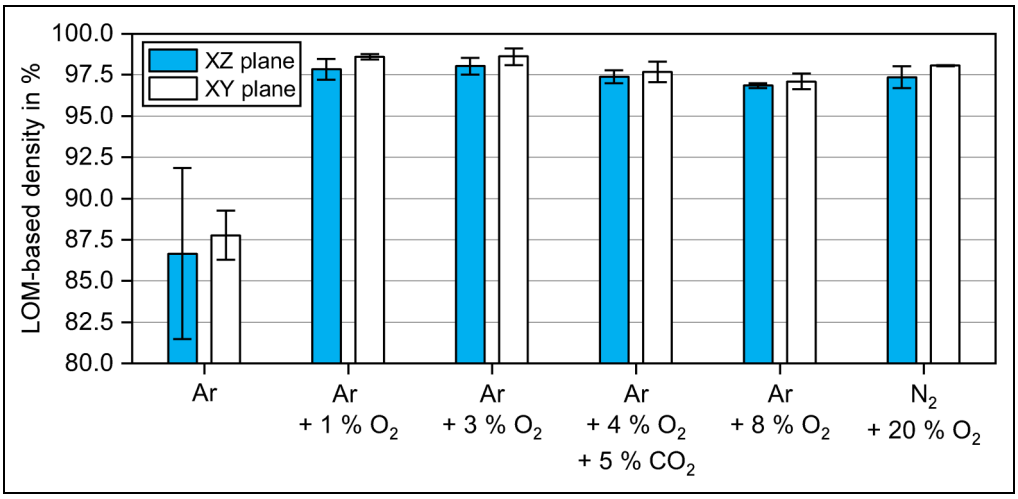

Figure 4. Densities based on light optical microscopy (LOM) of samples debinded in atmospheres with different oxygen contents at 300°C for 2 h and sintered in Argon at 1300°C for 2 h.

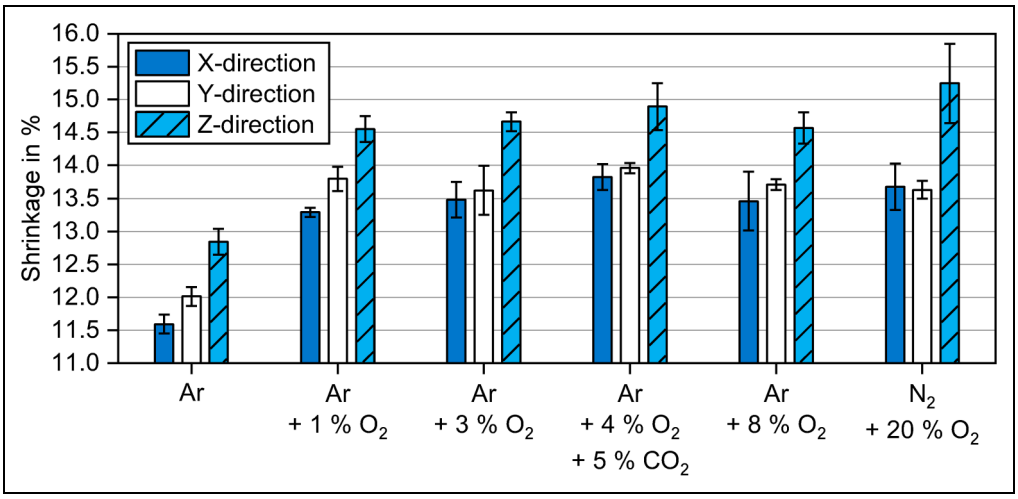

Figure 5. Shrinkages of samples debinded at 300°C for 2 h in atmospheres with different oxygen content and subsequently sintered in Ar at 1300°C for 2 h.

different amount of binder residues affects the phases present in the microstructure after sintering, hence influencing the overall bulk density. Another limitation originated from measurements with a micrometre screw gauge, which might be impacted by the surface roughness and not perfectly parallel planes of the cuboid samples.

Anisotropy of shrinkage was evident for all samples. The shrinkage in the *Z* direction (build direction) was more than 1% higher than in the *X* direction. The shrinkage in the *Y* direction tended to be slightly higher than in the *X* direction. Even though the shrinkage in the *Z* direction was higher than in the *X* or *Y* direction, the overall porosity in the *XZ* plane was still higher than in the *XY* plane.

Anisotropy during sintering is caused by density gradients in the green part, which are generated during the layerwise printing process.[24–27] Higher porosity generated between deposited layers in the build direction results in higher shrinkage. The observed differences in shrinkage along the *X* and *Y* direction can be attributed to the inhomogeneous powder packing created during the printing process. Zago et al.[30] argued that the binder droplet deposition creates an inhomogeneous porosity distribution in the powder layer. A ballistic effect of the binder droplets was observed by Parab et al.[31] using high-speed synchrotron X-ray imaging, which revealed particles ejected from the powder bed upon binder impact. It should be noted, however, that the induced porosity inhomogeneities depend on the technology used for powder spreading and binder deposition.

Bulk chemistry of sintered samples

The carbon and oxygen contents for samples sintered in Ar are compared in Figure 6 after debinding at 300°C for 2 h in atmospheres with varying oxygen content. Note that the carbon contents were based on the measurements from one sample, while the oxygen contents were based on multiple samples from different sintering runs, which explains the higher standard deviations in the case of oxygen.

Debinding in Ar led to significantly lower oxygen contents of 19 ppm compared to debinding performed in the oxygen-containing atmospheres. With 3 vol.% O_2 and higher, the final oxygen content was around ~2000 ppm. In comparison to that, debinding in 1 vol.% O_2 led to a considerably lower oxygen content of 627 ppm. The standard deviations in the oxygen values for each debinding atmosphere can be caused by oxidation during furnace cooling, the random placement of samples against the gas stream (difference in reducing potential during sintering) and slight temperature variations in the hot zone of the furnace. Nevertheless, the same trends of the debinding atmospheres were observed for all sintering cycles.

The carbon content after sintering was the highest at 2244 ppm when debinding took place in inert Ar. When debinded in Ar + 1 vol.% O_2, the carbon content dropped to 221 ppm after sintering. Using processing gas with 3 vol.% O_2 and above in the debinding atmosphere resulted in slightly lower carbon contents between 64 ppm and 99 ppm. The nitrogen values of all sintered samples decreased considerably to the level between 18 ppm and 50 ppm. All hydrogen values were below 2 ppm after sintering.

To better understand how the material chemistry changed from virgin powder to final sintered part, the evolutions of oxygen and carbon content from brown to sintered part are plotted in Figure 7 for the different debinding atmospheres. The bulk carbon and oxygen contents of the brown parts are a combination of residual binder and powder. The brown parts debinded in Ar and Ar + 1 vol.% O_2 resulted in higher bulk oxygen contents than for debinding in 3 vol.% O_2 up to 20 vol.% O_2 due to added oxygen by a higher amount of residual binder. The higher residual binder content is further supported by the higher carbon content of the brown parts in the case of Ar and Ar + 1 vol.% O_2. The chemistry of the brown parts is discussed in more detail in part I of the study.[23]

A significant reduction in bulk oxygen from brown to sintered samples is evident in all cases, see Figure 7(a). For debinding in 3 vol.% O_2 up to 20 vol.% O_2, the

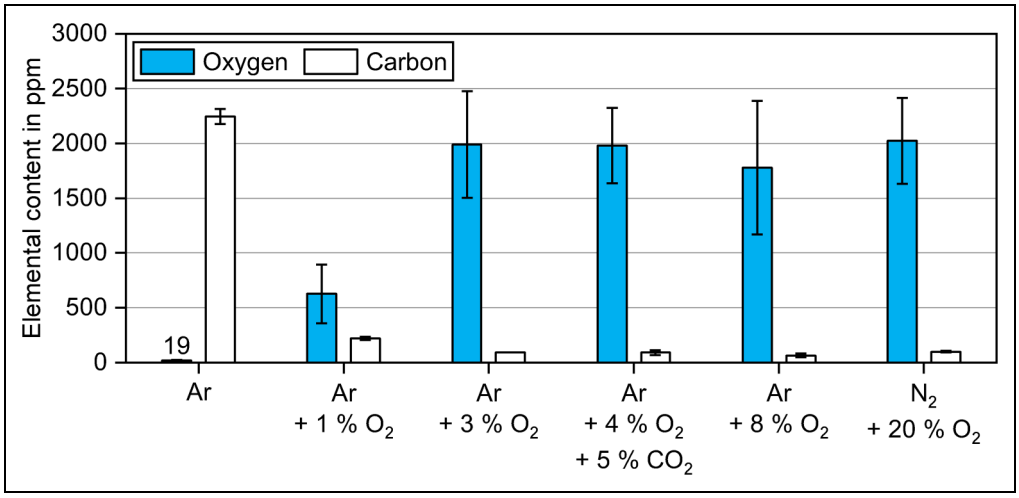

Figure 6. Oxygen and carbon contents of samples sintered in Ar after debinding at 300°C for 2 h in atmospheres with different oxygen contents.

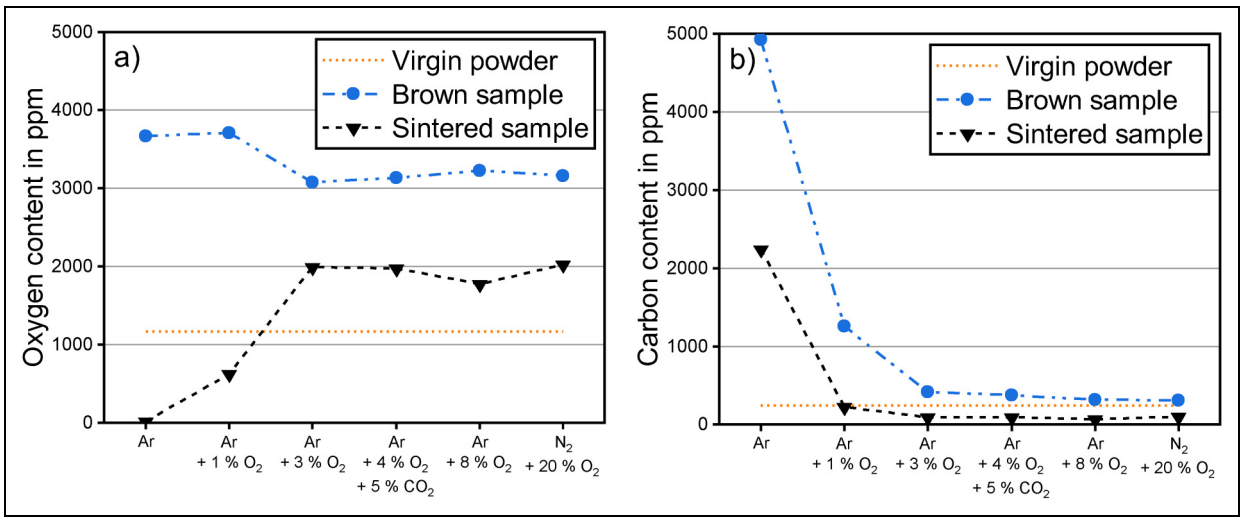

Figure 7. Evolution of (a) oxygen content and (b) carbon content from brown to sintered part for debinding at 300°C for 2 h in atmospheres with different oxygen content.

remaining binder content in the brown part was minor.[23] Therefore, the loss of oxygen was mainly connected to the deoxidation of the 17-4 PH powder. Nevertheless, the final oxygen contents were between 614 ppm and 858 ppm higher than in the virgin powder, which amounted to an increase of 53% to 74%.

When debinding and sintering were performed in Ar, the excess oxygen from the binder and nearly all oxygen from the virgin powder were completely removed. For debinding in 1 vol.% O_2, the oxygen removal was substantially higher than for debinding in 3 vol.% O_2 up to 20 vol.% O_2. While some removed oxygen for 1 vol.% O_2 originated from the higher binder content in the brown sample, the final oxygen content was reduced significantly by 46% compared to the initial virgin powder level. Even though oxygen contents of sintered 17-4 PH stainless steel are not specified in industry standards, lower oxygen levels in stainless steels are generally preferred due to the detrimental impact of oxide inclusions on mechanical performance and corrosion properties.[8,32]

The chemical evolution of the carbon content is highlighted in Figure 7(b). The carbon content of the sintered parts can be used to evaluate the quality of the thermal debinding process.[33] If the carbon content is higher than in the initial powder, the binder was not completely removed.[33] For debinding in Ar, a considerable drop in carbon from brown to sintered part was measured, but the final carbon content was substantially higher than in the virgin powder. For debinding in 1 vol.% O_2, the initial powder carbon content was reached in the as-sintered samples. For higher oxygen contents in the debinding atmosphere, the carbon contents dropped even below the virgin powder level, which indicated decarburisation of the 17-4 PH material.

All debinding atmospheres, except Ar, fulfilled the carbon requirement of MPIF 35 and ASTM B883-24 standard, which define a maximum carbon level of 0.07 wt.% (700 ppm).[28,29] A carbon content below 0.1 wt.% is preferred for 17-4 PH to achieve good strength, hardness and corrosion properties.[6–8] A very low carbon content in stainless steels ensures a lower probability for the precipitation of Cr-rich carbides.[33] Cr-rich carbides lead to a local depletion of Cr in the matrix, which makes these areas more susceptible to corrosion.[32,33] For press and sinter parts, a carbon content of 0.02 to 0.04 wt.% provides an optimum combination of sintered strength and ductility.[34] The latter carbon content range was achieved only for debinding in 1 vol.% O_2.

In summary, debinding and sintering in Ar resulted in nearly no oxygen content after sintering but excessive carbon content originating from insufficient binder removal. While debinding in 3 vol.% O_2 up to 20 vol.% O_2 led to efficient carbon removal even below the initial virgin powder level, the material picked up undesirable oxygen compared to the virgin powder. A combination of limited carbon pickup and oxygen reduction in the as-sintered part compared to the virgin powder was achieved by debinding in 1 vol.% O_2.

Oxygen and carbon loss during sintering

The analysis of the weight ratio of oxygen and carbon removed during sintering can potentially provide more insight into how these elements were removed. The calculated mass losses of oxygen and carbon from brown parts to sintered parts are plotted in Figure 8 for the different debinding atmospheres. The corresponding weight ratio of oxygen to carbon is indicated in the graph.

The weight losses revealed that the ratio of removed oxygen to carbon increased with increasing oxygen content in the debinding atmosphere. The ratio of carbon to oxygen removed during sintering after debinding in Ar was 1.4:1. The mass ratio of elemental oxygen to carbon is ~1.3:1 (16:12). While the carbon removed was mostly introduced by the binder, the oxygen loss was a combination of the removed binder and the oxide reduction of the 17-4 PH stainless steel. For debinding in 1 vol.% O_2,

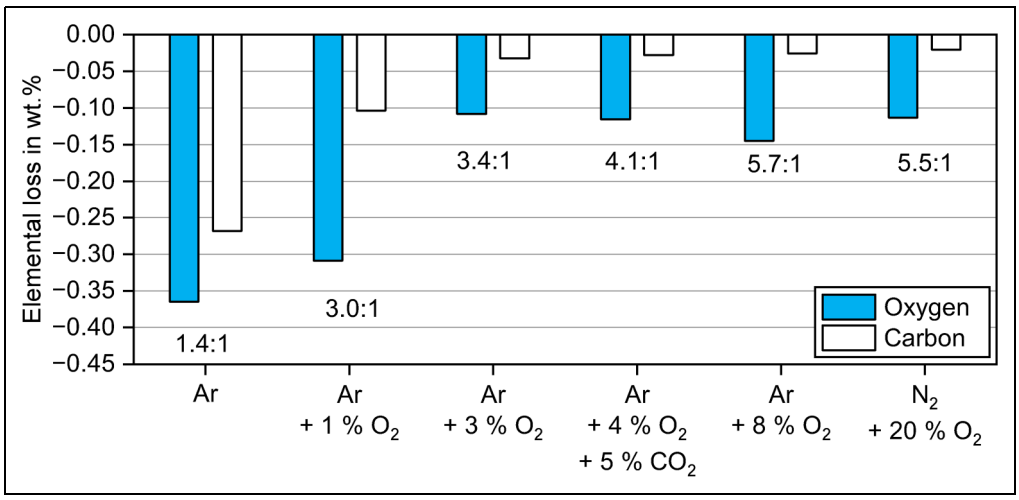

Figure 8. Weight ratio of oxygen and carbon removed from brown to sintered part for debinding in atmospheres with different oxygen content.

the oxygen/carbon loss ratio increased to 3.0:1 even though the initial binder content in the brown part was lower as seen in Figure 7. Similar to debinding in Ar, the oxygen removal was caused by a loss of binder and by reduction of metal oxides.

The weight ratio of oxygen loss to carbon loss increased up to 5.7:1 for debinding in 3 vol.% O_2 to 20 vol.% O_2. In the brown samples for debinding in 3 vol.% O_2 up to 20 vol.% O_2, most added oxygen in contrast to the powder stemmed from the oxidised 17-4 PH powder as described in detail in part I of this study,[23] whereas additional carbon compared to the virgin powder originated from binder residues on the powder surfaces.

While some oxygen loss was caused by the removal of the binder, sintering led to a considerable decrease in oxygen for all debinding atmospheres compared to the brown parts. Since sintering was conducted in inert Ar without providing any additional reducing agent such as hydrogen in the surrounding atmosphere, the deoxidation of the metal can occur by oxide dissociation, which is described as follows:

$$\frac{2}{y}\mathrm{M}_x\mathrm{O}_y \leftrightarrow \frac{2x}{y}\mathrm{M} + \mathrm{O}_2$$

The dissociation of metal oxides, however, requires a low oxygen partial pressure to thermodynamically occur and strongly depends on the stability of the oxide. The minimum required oxygen partial pressures for the reduction of iron oxides such as FeO, Fe_2O_3, Fe_3O_4 at 1300°C are between $\sim 10^{-8}$ bar and $\sim 10^{-11}$ bar.[35] It becomes even more challenging for more stable metal oxides such as Cr_2O_3 requiring oxygen partial pressures below $\sim 10^{-15}$ bar at 1300°C.[35] In practice, the required oxygen partial pressure for the dissociation of stable oxides such as SiO_2, MnO and $FeCr_2O_4$ cannot be achieved in industrial vacuum sintering furnaces. The oxygen partial pressure in the atmospheric furnace in this study was 10^{-5} bar (10 ppm O_2 at 1 bar). Therefore, dissociation of the metal oxides was unlikely during sintering.

As deoxidation occurred during sintering, the reduction of metal oxides could only be achieved by a reducing agent provided by the binder or its gaseous decomposition products. Insufficient debinding can result in binder residues. The decomposition of the binder residues at elevated temperatures can lead to the formation of amorphous carbon on the powder surface.[36] This carbon can further reduce metal oxides by carbothermal reduction reactions. A distinction is made between direct and indirect carbothermal reduction.

The direct carbothermal reduction of a metal oxide is the reaction with elemental carbon forming carbon monoxide (CO).[2] Direct carbothermal reduction requires direct contact between solid carbon and metal oxides. The direct carbothermal reduction can be generally defined as:

$$\frac{2}{y}\mathrm{M}_x\mathrm{O}_y + 2\mathrm{C} \leftrightarrow \frac{2x}{y}\mathrm{M} + 2\mathrm{CO}$$

The indirect carbothermal reduction of a metal oxide is the reaction with CO to form carbon dioxide (CO_2).[2] The CO can be provided by a process gas or be formed as reaction products of direct carbothermal reaction. The corresponding reaction can be universally described as:

$$\frac{2}{y}\mathrm{M}_x\mathrm{O}_y + 2\mathrm{CO} \leftrightarrow \frac{2x}{y}\mathrm{M} + 2\mathrm{CO}_2$$

The direct and indirect carbothermal reduction are interlinked by the Boudouard equilibrium defined as:

$$\mathrm{C} + \mathrm{CO}_2 \leftrightarrow 2\mathrm{CO}$$

According to the Boudouard equilibrium, the direct carbothermal reduction occurs thermodynamically at temperatures above ~720°C, when the equilibrium is shifted to the formation of CO.[12] The direct carbothermal reduction is registered experimentally at temperatures above ~900°C for Fe-Cr-based PM steels.[37] The obtained CO can then further reduce iron oxides to form CO_2 according to the indirect carbothermal reduction. The indirect carbothermal reduction is considered the dominating mechanism

because of the higher reaction kinetics related to a gaseous agent (CO) in comparison to solid carbon.[11] Close to the sintering temperature, the reduction of complex internal oxides by carbon dissolved in the metal occurs.[12]

The influence of carbothermal reduction on the sintering of steels has been well studied for PM steels, where graphite is admixed to the powder compacts.[2,11,12,37,38] Graphite is used as a carbon source in PM components to control the final carbon and oxygen content in sintered components. Carbothermal reduction is the main reduction mechanism for stable oxides at high sintering temperatures such as Cr oxides.[5]

In the case of BJT, the binder is directly deposited onto the powder surfaces during printing. Therefore, the residual binder after debinding is directly located on the powder surfaces and acts as a source of carbon. This likely results in direct carbothermal reduction during the heating stage followed by indirect carbothermal reduction by CO. The direct and indirect carbothermal reduction contribute in parallel to the oxide removal during sintering. Yang et al.[39] reported for BJT of water-atomised low-alloy steel that carbon residue from the binder decomposition enhanced the oxide removal at higher temperatures.

When debinding was conducted in Ar, a portion of the 0.47 wt.% carbon residue from the binder can be assumed to directly contribute to the oxide reduction as elemental carbon. The carbon content in the brown sample was much higher than the oxygen content, see Figure 7. Even after the full removal of oxygen by carbothermal reduction, a high portion of carbon was still present in the as-sintered sample. For debinding in 1 vol.% O_2, the additional carbon of 0.10 wt.% in the brown part compared to the virgin powder resulted in significant deoxidation of the 17-4 PH stainless steel during sintering by carbothermal reduction while resulting in no carbon pickup.

When debinding was performed in 3 vol.% O_2 up to 20 vol.% O_2, the carbon content in the brown part was slightly higher than in the virgin powder, indicating that some carbon was dissolved during sintering. Therefore, less elemental carbon could form to enable carbothermal reduction during sintering. Nevertheless, some deoxidation of the material took place during sintering. Since the carbon content dropped below the virgin powder level after sintering, decarburisation occurred by consuming carbon stemming from the powder for reduction reactions.

It was shown that both the starting oxygen and carbon content before sintering have a significant impact because oxygen and carbon interact during sintering.[6] The binder residue and powder oxidation during the debinding had a direct impact on the final carbon and oxygen content after sintering. In conclusion, a beneficial effect of the remaining binder on oxide reduction of 17-4 PH stainless steel BJT parts was demonstrated. By tailoring the oxygen content in the debinding atmosphere, the binder removal and oxide reduction during sintering can be fine tuned. Debinding in Ar + 1 vol.% O_2 and sintering in Ar achieved the best balance of oxide reduction and no carbon pickup in the material during sintering.

Impact of debinding atmosphere composition on as-sintered micro-structure

To explain the differences in sintering densification for the different debinding atmospheres, the microstructure of the 17-4 PH samples was examined. The etched microstructures of the sintered 17-4 PH specimen for the *XZ* plane are shown in Figure 9 for the different debinding atmospheres. *XZ* planes are highlighted as the porosities were the highest due to the layer-wise printing process.

After debinding and sintering in Ar, the microstructure revealed a martensitic microstructure with the presence of pores. Martensite is known to form upon cooling of 17-4 PH from the sintering temperature.[8] Due to the high Ni content in the steel, martensite is obtained even at low cooling rates.[40] The presence of small fractions of retained austenite should be considered, but cannot be clearly observed by optical microscopy.[33]

When debinding was performed in oxygen-containing gas mixtures, the porosity decreased visibly. Furthermore, the microstructures revealed the presence of δ-ferrite in contrast to debinding in Ar. The δ-ferrite was located mainly along prior austenite grain boundaries and is referred to as island-type ferrite.[41] The formation of δ-ferrite is favoured at interparticle boundaries and pore surfaces due to the lower energy barrier for nucleation. Its fraction increases with increasing sintering temperature and hold time. Huber et al.[26] showed for BJT of 17-4 PH comparable densities of ~97% and microstructures with δ-ferrite after sintering at 1300°C for 30 min in H_2.

The nucleation of δ-ferrite during the sintering process enhances the sintering activity significantly. The reason for that is the higher rate of grain boundary and volume diffusion in the body-centred cubic crystal structure of δ-ferrite compared to the face-centred cubic crystal structure of γ-austenite.[42] The low densification after debinding in Ar was, therefore, connected to the absence of δ-ferrite enhancing the diffusion mechanisms during sintering. The positive effect of δ-ferrite on the sintering densification of 17-4 PH stainless steel was reported in several studies.[42–44]

The phases present during sintering are heavily dependent on the alloy composition and the sintering temperature. This is demonstrated in the quasi-binary phase diagram of 17-4 PH stainless steel in Figure 10(a) calculated for the alloy composition of the used powder (Fe-17.77Cr-4.15Ni-3.95Cu-0.56Si-0.46Mn-C) in this work. The two-phase region δ+γ for solid-state sintering extends to a maximum of 0.23 wt.% carbon at 1359°C. For carbon levels up to 0.3 wt.%, a liquid phase might be present for temperatures above 1337°C. Small fractions of liquid phase are beneficial for sintering densification which is referred to as supersolidus–liquid phase sintering. Excessive liquid phase formation, however, causes problems in shape retention during sintering.

Carbon has a crucial impact on whether δ-ferrite is thermodynamically stable during sintering. Considering the sintering temperature of 1300°C, the nucleation of δ-ferrite can only be expected for carbon contents below 0.16 wt.%. This was in accordance with the measured

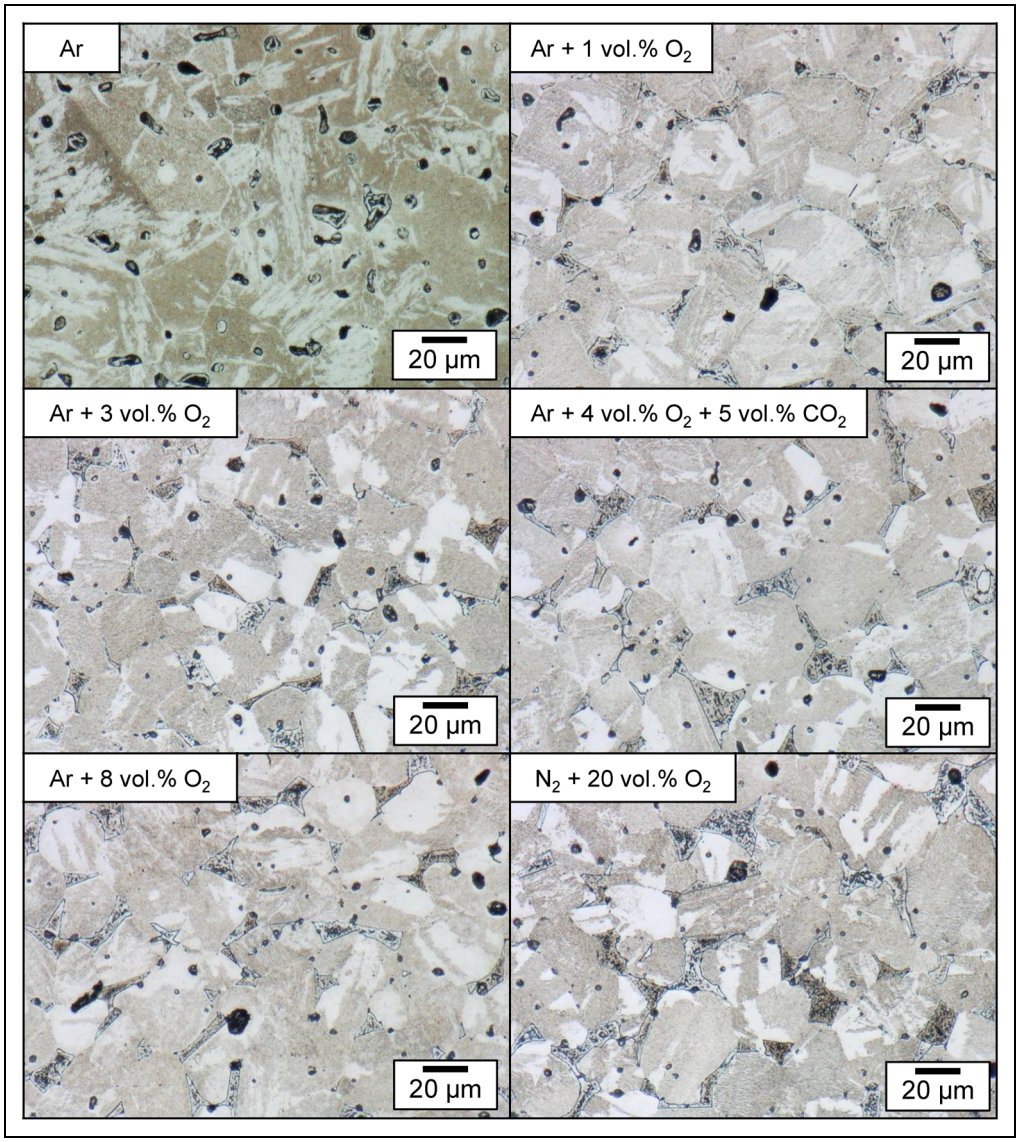

Figure 9. Etched microstructure of 17-4 PH parts debinded in atmospheres with different oxygen content and sintered at 1300°C in Ar.

carbon content of 0.22 wt.% after debinding and sintering in Ar, where no δ-ferrite was observed in the final microstructure combined with low densification after sintering. Inversely, the as-sintered samples with low carbon content after debinding in oxygen-containing atmospheres, which were close to the virgin powder content of 245 ppm, showed δ-ferrite in the microstructure after sintering as predicted by the phase diagram.

The amount of δ-ferrite formed at any given temperature is affected by the carbon content. The equilibrium volume fractions of phases present at the sintering temperature of 1300°C are plotted in Figure 10(b) in dependence on the carbon content. Below the carbon threshold value for δ-ferrite formation, the volume fraction of δ-ferrite increases with decreasing carbon levels until a maximum of 30 vol.% because carbon is a strong γ-austenite stabiliser. The carbon contents of sintered samples after debinding in Ar and after debinding in an oxygen-containing atmosphere are indicated in Figure 10(b) by a dotted line. At equilibrium conditions at 1300°C, the microstructure would consist of ∼25 vol.% δ-ferrite and ∼75 vol.% γ-austenite for 221 ppm of carbon after debinding in 1 vol.% O_2. For debinding in 3 vol.% O_2 up to 20 vol.% O_2, the δ-ferrite amount would slightly increase to 28 vol.% for 99 ppm of carbon. While the δ-ferrite will also partially transform to austenite and martensite during cooling, the austenite phase is typically transformed into martensite during cooling from the sintering temperature. Retained austenite might still be present.

Conclusions

The impact of oxygen content in the processing atmosphere during the debinding of BJT green parts on the sintering of 17-4 PH stainless steel was investigated. A previous study compared the binder residue in brown parts and the powder oxidation after debinding in atmospheres with varying oxygen content.[23] In this work, the

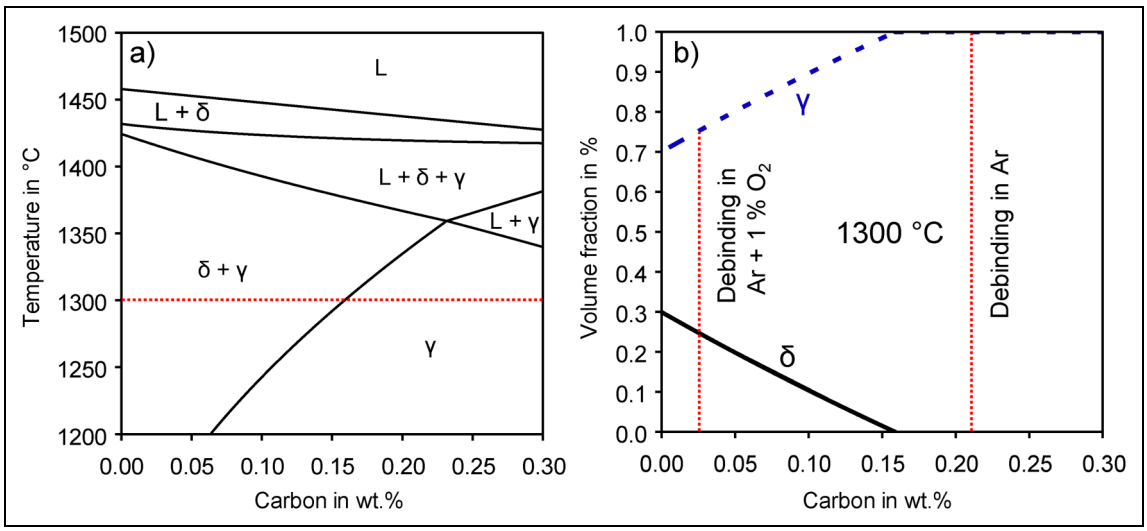

Figure 10. (a) Quasi-binary phase diagram of 17-4 PH (Fe-17.77Cr-4.15Ni-3.95Cu-0.56Si-0.46Mn-C) and (b) volume fractions of phases at 1300°C depending on the carbon content.

obtained brown parts were sintered at 1300°C for 2 h in an inert Ar atmosphere. The influence of the debinding atmosphere was analysed by comparing density, shrinkage, chemistry and microstructure after sintering. The evolution of the carbon and oxygen content from the virgin powder over the brown part to the sintered part was thoroughly discussed.

Samples debinded in inert Ar led to the lowest sintered densities of ~88% and the lowest shrinkages in contrast to samples debinded in oxygen-containing atmospheres. The microstructure revealed high porosity and the absence of δ-ferrite. The δ-ferrite phase was not formed during sintering due to the high carbon content of 0.22 wt.% originating from insufficient binder removal during the debinding step. Thermodynamic calculations confirmed that no δ-ferrite formation at 1300°C was expected for carbon contents above 0.16 wt.%. The high carbon pickup resulted, however, in nearly complete oxide removal during sintering by carbothermal reduction. The final oxygen content was 19 ppm compared to the virgin powder content of 1163 ppm.

Debinding in Ar + 1 vol.% O_2 resulted in significantly higher densities of ~98% and higher shrinkages after sintering compared to debinding in Ar. The microstructure exhibited δ-ferrite distributed along prior austenite grain boundaries. The higher diffusivity in the body-centred cubic crystal structure of ferrite compared to the face-centred cubic crystal structure of austenite caused considerably higher densification during sintering. The formation of the δ-ferrite phase was predicted during sintering for a carbon content of 221 ppm with an equilibrium phase fraction of ~25 vol.% at 1300°C. The final oxygen content after sintering was 627 ppm, which was substantially reduced by 46% compared to the virgin powder. The added carbon content by the binder of 0.10 wt.% in the brown samples was efficient in reducing high fractions of oxides on the powder surface while no carbon pickup in the sintered material was measured.

When green parts were debinded in Ar + 3 vol.% O_2, Ar + 4 vol.% O_2 + 5 vol.% CO_2, Ar + 8 vol.% O_2 and N_2 + 20 vol.% O_2, the sintered parts exhibited similar densities and chemistry. The densities after sintering were comparable to debinding in 1 vol.% O_2 ranging from 96% to 98%. The corresponding microstructures revealed the presence of δ-ferrite responsible for the higher sintering densification compared to debinding in Ar. The 17-4 PH material showed a significant oxygen increase between 614 and 858 ppm after sintering compared to the virgin powder. While oxygen reduction was measured from the brown to the sintered part in all cases, the low amount of binder residues in the brown part did not enable the reduction of the oxygen picked up during debinding.

It was demonstrated that tailoring the oxygen content in the atmosphere can achieve an improved material chemistry for 17-4 PH stainless steel after sintering in Ar at 1300°C. When debinding was performed in Ar + 1 vol.% O_2, a low amount of carbon originating from the binder was effective in deoxidation of the material without inhibiting the formation of δ-ferrite for enhanced densification during sintering.

Acknowledgments

This work was conducted in the framework of the Centre for Additive Manufacturing – Metal (CAM^2), supported by the Swedish Governmental Agency of Innovation Systems (Vinnova). Linde GmbH acknowledges the funding by the Federal Ministry of Research and Education (BMBF, Germany) for the project SINEWAVE (FKZ 03HY123A) within the Hydrogen Flagship Project H2Giga. The authors acknowledge the contribution of Mumtahena Shahabuddin Jim for carrying out parts of the experimental work.

Declaration of conflicting interests

The authors declared no potential conflicts of interest with respect to the research, authorship, and/or publication of this article.

Funding

The authors disclosed receipt of the following financial support for the research, authorship, and/or publication of this article: This work was supported by the Swedish Governmental Agency of Innovation Systems (Vinnova) with grant number 2016-05175 and the Federal Ministry of Research and Education (BMBF) under SINEWAVE (FKZ 03HY123A).

ORCID iD

Kai Zissel https://orcid.org/0000-0001-7996-1979

References

1. Mirzababaei S and Pasebani S. A review on binder jet additive manufacturing of 316L stainless steel. *J Manuf Mater Process* 2019; 3: 82.
2. Gierl-Mayer C. Reactions between ferrous powder compacts and atmospheres during sintering – an overview. *Powder Metall* 2020; 63: 1–17.
3. Shen H, He H, Zou J, et al. Effects of high oxygen content on the densification behavior of 316L stainless steel during the later sintering stage. *JOM* 2023; 75: 2543–2553.
4. German RM and Bose A Binder removal. In: *Binder and polymer assisted powder processing*. Novelty, OH: ASM International, 2020, pp. 139–167.
5. Hryha E and Nyborg L. Thermogravimetry study of the effectiveness of different reducing agents during sintering of Cr-prealloyed PM steels. *J Therm Anal Calorim* 2014; 118: 825–834.
6. German RM. MIM 17-4 PH stainless steel: processing, properties and best practice. *Powder Injection Mould Int* 2018; 12(2): 49–76.
7. Baba T, Miura H, Honda T, et al. Properties of 17-4 PH stainless steels produced by metal injection Molding process. *J Jpn NSociety Powder Powder Metall* 1995; 42: 1119–1123.
8. German RM and Bose ACase studies of powder-binder processing practices. In: *Binder and polymer assisted powder processing*. Novelty, OH: ASM International, 2020, pp. 201–249.
9. Washko SD and Aggen G. Wrought stainless steels. In: ASM Handbook Committee (ed.) *Properties and selection: irons, steels, and high-performance alloys*. Novelty, OH: ASM International, 1990, pp. 841–907.
10. Hryha E, Borgström H, Sterky K, et al. Influence of the steel powder type and processing parameters on the debinding of PM compacts with gelatin binder. *J Therm Anal Calorim* 2014; 118: 695–704.
11. De Oro Calderon R, Gierl-Mayer C and Danninger H. Application of thermal analysis techniques to study the oxidation/reduction phenomena during sintering of steels containing oxygen-sensitive alloying elements. *J Therm Anal Calorim* 2017; 127: 91–105. doi:10.1007/s10973-016-5508-5.
12. Hryha E, Dudrova E and Nyborg L. On-line control of processing atmospheres for proper sintering of oxidation-sensitive PM steels. *J Mater Process Technol* 2012; 212: 977–987.
13. Tan Z, Engström U, Li K, et al. Effect of furnace atmosphere on sintering process of chromium-containing steel via powder metallurgy. *J Iron Steel Res Int* 2021; 28: 889–900.
14. Chasoglou D, Hryha E and Nyborg L. Effect of process parameters on surface oxides on chromium-alloyed steel powder during sintering. *Mater Chem Phys* 2013; 138: 405–415.
15. Kremel S, Danninger H and Yu Y. Effect of sintering conditions on particle contacts and mechanical properties of pm steels prepared from 3%cr prealloyed powder. *Powder Metall Prog* 2002; 2: 211–221.
16. Oro R, Campos M, Gierl-Mayer C, et al. New alloying systems for sintered steels: critical aspects of sintering behavior. *Metall Mater Trans A* 2015; 46: 1349–1359.
17. Gierl-Mayer C, de Oro Calderon R and Danninger H. The role of oxygen transfer in sintering of low alloy steel powder compacts: a review of the "internal getter" effect. *JOM* 2016; 68: 920–927.
18. Danninger H, De Oro Calderon R and Gierl-Mayer C. Oxygen transfer reactions during sintering of Ferrous powder compacts. *Adv Eng Forum* 2018; 27: 3–13.
19. Gierl-Mayer C, de Oro Calderon R and Danninger H. Sintering of ferrous metallic compacts: chemical reactions that involve interstitial elements. *J Am Ceram Soc* 2019; 102: 695–705.
20. de Oro Calderon R, Gierl-Mayer C and Danninger H. Thermoanalytical techniques for characterizing sintering processes in ferrous powder metallurgy. *J Therm Anal Calorim* 2023; 148: 1309–1320.
21. Danninger H and Gierl C. Processes in PM steel compacts during the initial stages of sintering. *Mater Chem Phys* 2001; 67: 49–55.
22. Danninger H, Xu C and Lindqvist B. Oxygen removal during sintering of steels prepared from Cr-Mo and Mo prealloyed powders. *Mater Sci Forum* 2007; 534–536: 577–580.
23. Zissel K, Quejido EB, Forêt P, et al. Impact of oxygen content on debinding of binder jetted 17-4 PH stainless steel parts: Part I – debinding. *Powder Metall* 2024.
24. Cabo Rios A, Hryha E, Olevsky E, et al. Sintering anisotropy of binder jetted 316L stainless steel: part II – microstructure evolution during sintering. *Powder Metall* 2022; 65(4): 283–295.
25. Cabo Rios A, Hryha E, Olevsky E, et al. Sintering anisotropy of binder jetted 316L stainless steel: part I – sintering anisotropy. *Powder Metall* 2021; 65(4): 273–282.
26. Huber D, Vogel L and Fischer A. The effects of sintering temperature and hold time on densification, mechanical properties and microstructural characteristics of binder jet 3D printed 17-4 PH stainless steel. *Addit Manuf* 2021; 46: 102114.
27. Emanuelli L, Segata G, Perina M, et al. Study of microstructure and mechanical properties of 17-4 PH stainless steel produced via binder jetting. *Powder Metall* 2023; 66(5): 377–386.
28. Metal Powder Industries Federation. MPIF standard 35 – structural parts. 2018.
29. B09 Committee. *Standard Specification for metal injection molded (MIM) materials*. ASTM B883-24, https://www.astm.org/b0883-24.html (accessed 24 April 2024).
30. Zago M, Lecis N, Mariani M, et al. Analysis of the causes determining dimensional and geometrical errors in 316L and 17-4PH stainless steel parts fabricated by metal binder jetting. *Int J Adv Manuf Technol* 2024; 132: 835–851.
31. Parab ND, Barnes JE, Zhao C, et al. Real time observation of binder jetting printing process using high-speed X-ray imaging. *Sci Rep* 2019; 9: 2499.
32. Samal PK. Corrosion resistance of powder metallurgy stainless steels. In: Samal P and Newkirk J (eds) *Powder metallurgy*. Novelty, OH: ASM International, 2015, pp. 447–457.

33. Schroeder R, Hammes G, Binder C, et al. Plasma debinding and sintering of metal injection moulded 17-4PH stainless steel. *Mater Res* 2011; 14: 564–568.
34. Samal PK and Nandivada N. Properties of 17-4 PH stainless steel produced via press and sinter route In*:* PM2008 World Congress. Washington, USA. June 2008.
35. Karamchedu S. *Critical aspects of delubrication and sintering of chromium-alloyed powder metallurgy steels*. Gothenburg, Sweden: Chalmers University of Technology, 2015, https://research.chalmers.se/en/publication/220049 (accessed 20 February 2023).
36. Lou J, Liu M, He H, et al. Investigation of decarburization behaviour during the sintering of metal injection moulded 420 stainless steel. *Metals* 2020; 10: 211.
37. Hryha E, Karamchedu S, Riabov D, et al. Effect of active components of sintering atmosphere on reduction/oxidation processes during sintering of Cr-alloyed PM steels. *J Am Ceram Soc* 2015; 98: 3561–3568.
38. Danninger H, de Oro Calderon R and Gierl-Mayer C. Chemical reactions during sintering of PM steel compacts as a function of the alloying route. *Powder Metall* 2018; 61: 241–250.
39. Yang M, Keshavarz MK, Vlasea M, et al. Supersolidus liquid phase sintering of water-atomized low-alloy steel in binder jetting additive manufacturing. *Heliyon* 2023; 9: e13882.
40. Sha W, Leitner H, Guo Z, et al. 11 - Phase transformations in maraging steels. In: Pereloma E and Edmonds DV (eds) *Phase transformations in steels*. Cambridge, UK: Woodhead Publishing, 2012, pp. 332–362.
41. Radhakrishnan J, Kumar P, Gan SS, et al. Microstructure and tensile properties of binder jet printed 17–4 precipitation hardened martensitic stainless steel. *Mater Sci Eng A* 2022; 860: 144270.
42. Wu Y, Blaine D, Schlaefer C, et al. Sintering densification and microstructural evolution of injection molding grade 17-4 PH stainless steel powder. *Metall Mater Trans A* 2002; 33: 2185–2194.
43. Kazior J. Influence of sintering atmosphere, temperature and the solution-annealing treatment on the properties of precipitation-hardening sintered 17-4 PH stainless steel. *Materials* 2023; 16: 760.
44. Wu Y, Blaine D, Marx B, et al. Effects of residual carbon content on sintering shrinkage, microstructure and mechanical properties of injection molded 17-4 PH stainless steel. *J Mater Sci* 2002; 37: 3573–3583.